CHEMISTRY
A EUROPEAN JOURNAL

Decomposition of Neutral, Singly and Doubly Protonated Benzoquinone in the Gas Phase

Jana Roithová,[a, b] Detlef Schröder,*[a] and Helmut Schwarz[a]

Dedicated to Professor Assa Lifshitz on the occasion of his 70th birthday

Abstract: The unimolecular fragmentations of singly and doubly protonated *ortho*-, *meta*-, and *para*-benzoquinones (BQH^+ and BQH_2^{2+}, respectively) are studied by tandem mass spectrometry. The dominant fragmentation pathways lead to the elimination of a neutral CO molecule from BQH^+ and, by charge separation, to the expulsion of protonated CO from BQH_2^{2+}. Reaction mechanisms are elucidated based on labeling experiments and UB3LYP calculations. These results reveal that the respective reactions proceed in an analogous fashion to the decarbonylation of neutral benzoquinones, which decompose into carbon monoxide and cyclopentadienone. Single protonation facilitates all steps on the reaction pathway with neutral CO and *O*-protonated cyclopentadienone as final products. In contrast, double protonation leads to an increase of the barriers for the decomposition yielding $CO{\cdot}H^+$ and *O*-protonated cyclopentadienone. This major process of BQH_2^{2+} is accompanied by two minor channels, which lead to the elimination of neutral carbon monoxide and water, respectively. The proton affinity of the *para*-BQH^+ monocation is estimated as 3.6 ± 0.3 eV.

Keywords: density functional calculations · dications · electron-deficient compounds · protonation · quinones

Introduction

Benzoquinones (BQ), especially *para*-benzoquinone (**1**), operate as molecular building blocks for redox reagents in many biological systems.[1] Their function evolves from the ability to serve as efficient electron acceptors. In solution, *para*-benzoquinone can readily accept two electrons. The so-formed dianion couples with two protons to yield the hydroquinone molecule (*para*-BQH_2, **3**), for which a substantial driving force is the formation of the aromatic ring. This reasoning also implies that the oxidizing power is increased in acidic media, that is, when protonation precedes electron transfer. The experimental proton affinity of *para*-benzoquinone is 8.28 ± 0.09 eV[2] with the oxygen atom as the preferred protonation site. The electronic structures of *para*-benzoquinone (**1**) and *ortho*-benzoquinone (**4**) correspond to that of α,β-unsaturated ketones (see Scheme 1).[3] Calculations (B3LYP/6–31G*) have shown that the geometry of *para*-benzoquinone is not significantly changed upon single protonation (*para*-BQH^+, $\mathbf{2}^+$). The structural changes are quite comparable to those between the geometries of acetone and protonated acetone.[4]

We asked ourselves to what extent protonation influences the overall electronic structure of benzoquinones and thus the unimolecular reactivity. As there are two carbonyl moieties in the molecule, other questions also evolve. For example, are the doubly protonated benzoquinones thermodynamically stable? What are the proton affinities of the corresponding monocations BQH^+, and how does double protonation influence the electronic structures and the unimolecular reactivities of benzoquinones?

From the point of view of electronic structure, *ortho*-benzoquinone (**4**) should exhibit similar features to the *para*-compound **1**, whereas the so-far elusive *meta*-benzoquinone (**7**; see Scheme 2) is expected to be markedly different. On the basis of (σS,πSD)QCI/6–31G* calculations, the ground state of **7** has been predicted as a triplet with a strongly de-

[a] Dr. J. Roithová, Dr. D. Schröder, Prof. Dr. H. Schwarz
Institut für Chemie der Technischen Universität Berlin
10623 Berlin (Germany)
Fax: (+49) 30-314-21102
E-mail: detlef.schroeder@tu-berlin.de

[b] Dr. J. Roithová
V. Čermák Laboratory
J. Heyrovský Institute of Physical Chemistry,
Academy of Sciences, 18223 Praha 8 (Czech Republic)

Supporting information for this article is available on the WWW under http://www.chemeurj.org/ or from the author.

© 2005 Wiley-VCH Verlag GmbH & Co. KGaA, Weinheim
DOI: 10.1002/chem.200400738

localized wave function.[5] Thus, the family of benzoquinones represents an interesting system for stability and reactivity studies as a comparison of the various isomers can shed light also on the reactivity of the triplet states.

Results and Discussion

Proton affinity and stability: The proton affinity (PA) of *para*-BQH^+ ($\mathbf{2}^+$) can be determined by means of Born–Haber cycles. Considering reaction (1), the heat of formation (Δ_fH) of *para*-BQH^+ ($\mathbf{2}^+$) and Δ_fH of *para*-BQH_2^{2+} ($\mathbf{3}^{2+}$) have to be determined, whereas $\Delta_fH(H^+)$ is 15.86 eV at 298 K.[6,7]

$$\underset{\mathbf{2}^+}{para\text{-}BQH^+} + H^+ \rightarrow \underset{\mathbf{3}^{2+}}{para\text{-}BQH_2^{2+}} \quad (1)$$

$\Delta_fH(\mathbf{2}^+)$ can be derived from Δ_fH of *para*-benzoquinone (**1**), which is -1.24 ± 0.04 eV[8] and its known proton affinity, $PA(\mathbf{1})=8.28\pm0.09$ eV,[2] leading to $\Delta_fH(\mathbf{2}^+)$ of 7.04 ± 0.10 eV at 298 K. $\Delta_fH(\mathbf{3}^{2+})$ can be derived from $\Delta_fH(\mathbf{3})=-2.87\pm0.01$ eV,[9] and its first and second ionization energies, $IE(\mathbf{3})=7.94\pm0.01$ eV[6] and $IE(\mathbf{3}^+)=14.2\pm0.3$ eV (Table 1). This leads to a value for $\Delta_fH(\mathbf{3}^{2+})$ of 19.3 ± 0.3 eV at 298 K and thus to the desired proton affinity $PA(\mathbf{2}^+)=3.6\pm0.3$ eV at 298 K.

An analogous deduction is impossible for the *ortho* and *meta* isomers, $\mathbf{5}^+$ and $\mathbf{8}^+$, respectively, due to a lack of the necessary thermochemical data. However, proton affinities can be also obtained from calculations (Table 2). The corresponding theoretically derived value of $PA_{calcd}(\mathbf{2}^+)=3.74$ eV is in agreement within the error margins of the experimental value, thus showing the validity of the computational approach. For the *ortho* and *meta* isomers $\mathbf{5}^+$ and $\mathbf{8}^+$ the calculated proton affinities are 3.27 and 3.74 eV, respectively.

Table 1. Adiabatic ionization energies[a] (IE_a) of $\mathbf{3}^+$, $\mathbf{6}^+$, and $\mathbf{9}^+$ as determined by charge stripping.

	IE_a [eV]
$\mathbf{3}^+$ (*para*-BQH_2^+)	14.2 ± 0.3
$\mathbf{6}^+$ (*ortho*-BQH_2^+)	14.5 ± 0.2
$\mathbf{9}^+$ (*meta*-BQH_2^+)	14.7 ± 0.2

[a] A recent detailed analysis of the charge stripping of toluene cation $C_7H_8^+$ reveals that the Q_{min} value of $C_7H_8^+$ is associated with an adiabatic transition to the dication.[35] Considering the similarity of the calculated difference between vertical and adiabatic ionization energies ($\Delta E_{v/a}$) of $C_7H_8^+$ (0.33 eV), *ortho*-BQH_2^+ (0.38 eV), *meta*-BQH_2^+ (0.24 eV), and *para*-BQH_2^+ (0.31 eV), we therefore conclude that the Q_{min} values correspond also to adiabatic transitions within experimental error.

Table 2. Proton affinities (PAs) of **1**, $\mathbf{2}^+$, **4**, $\mathbf{5}^+$, **7**, and $\mathbf{8}^+$ as calculated by the UB3LYP/cc-pVTZ method.

	State	PA_{calcd} [eV]
1 (*para*-BQ)	$^1A_1$	8.38
$\mathbf{2}^+$ (*para*-BQH^+)	$^1A'$	3.74
4 (*ortho*-BQ)	$^1A_1$	8.71
$\mathbf{5}^+$ (*ortho*-BQH^+)	$^1A'$	3.27
7 (*meta*-BQ)	$^3B_2$	8.44
	^1A	10.12
$\mathbf{8}^+$ (*meta*-BQH^+)	$^3A'$	4.11
	$^1A'$	3.74

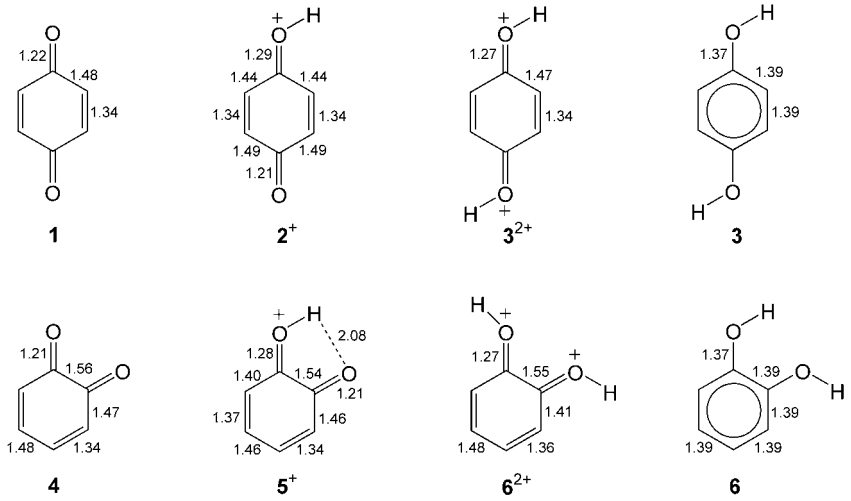

Scheme 1.

The unexpectedly large proton affinities of the BQH^+ monocations can be attributed to the relatively favorable electronic structures of the resulting dications BQH_2^{2+}. The *ortho* and *para* isomers $\mathbf{3}^{2+}$ and $\mathbf{6}^{2+}$, respectively, can be regarded as quinones with two protons attached to the carbonyl moieties of the neutral benzoquinones. This reasoning is also supported by the optimized geometries computed for the *para* and *ortho* dications (Scheme 1). The C–O bond lengths of the most stable conformers of $\mathbf{3}^{2+}$ and $\mathbf{6}^{2+}$ are 1.27 Å,[10] whereas the corresponding bond lengths in the neutral molecules, that is, *para*- and *ortho*-dihydroxybenzenes (**3** and **6**, respectively), are 1.37 Å. The C–C bonds of the rings of $\mathbf{3}^{2+}$ and $\mathbf{6}^{2+}$ exhibit bond alternations as in the case for the neutral BQ **1** and **4**, whereas the C–C bonds of the neutral molecules (**3** and **6**, respectively) have equal lengths of 1.39 Å.

The proton affinity of *ortho*-BQH^+ ($\mathbf{5}^+$) is 0.5 eV lower than that of the *para* isomer, which can be attributed to the interplay of two effects, one of which operates in the cation $\mathbf{5}^+$ and the other in the dication $\mathbf{6}^{2+}$. First, the *ortho* arrangement of the substituents in $\mathbf{5}^+$ permits an extra stabili-

 © 2005 Wiley-VCH Verlag GmbH & Co. KGaA, Weinheim

zation due to intramolecular hydrogen bonding (Scheme 1). This stabilizing effect is also reflected by the higher proton affinity of *ortho*-benzoquinone **4** ($PA_{calcd} = 8.71$ eV) compared to *para*-benzoquinone **1** ($PA_{calcd} = 8.38$ eV). Second, the *ortho* arrangement of the substituents in the dication $\mathbf{6}^{2+}$ brings the two protons close to each other, thus increasing the Coulomb repulsion in comparison to that in $\mathbf{3}^{2+}$ (Scheme 1).

As mentioned above, neutral *meta*-benzoquinone **7** has a triplet ($^3B_2$) ground state (Scheme 2, Table 3). Its electronic structure corresponds to a diradical with highly delocalized

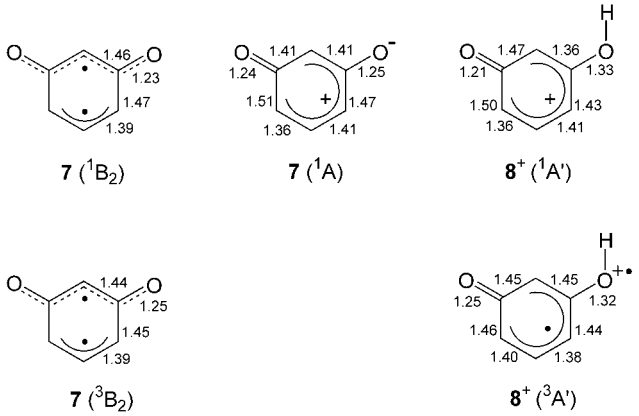

Scheme 2.

Table 3. Relative energies, E_{rel}, at 0 K of *para*-, *ortho*-, and *meta*-benzoquinones (**1**, **4**, and **7**, respectively), the protonated benzoquinones ($\mathbf{2}^+$, $\mathbf{5}^+$, and $\mathbf{8}^+$, respectively), and doubly protonated benzoquinones ($\mathbf{3}^{2+}$, $\mathbf{6}^{2+}$, and $\mathbf{9}^{2+}$, respectively).

	State	E_{rel} [eV]
1 (*para*-BQ)	$^1A_1$	0
	$^3B_1$	2.13
4 (*ortho*-BQ)	$^1A_1$	0.33
	$^3A''$	1.52
7 (*meta*-BQ)	$^3B_2$	1.23
	$^1B_2$	1.51
	^1A	2.20
$\mathbf{2}^+$ (*para*-BQH^+)	$^1A'$	0
	$^3A'$	1.05
$\mathbf{5}^+$ (*ortho*-BQH^+)	$^1A'$	0.00
	$^3A'$	0.97
$\mathbf{8}^+$ (*meta*-BQH^+)	$^1A'$	0.85
	$^3A'$	1.17
$\mathbf{3}^{2+}$ (*para*-BQH_2^{2+})	$^1A_1$	0
	$^3A''$	1.19
$\mathbf{6}^{2+}$ (*ortho*-BQH_2^{2+})	$^1A_1$	0.47
	$^3A''$	0.91
$\mathbf{9}^{2+}$ (*meta*-BQH_2^{2+})	$^1A_1$	0.85
	$^3B_2$	0.81

π electrons.[5] The electronic structure of the lowest lying singlet state $^1B_2$ (excitation energy of 0.28 eV) is similar, as reflected in the geometries (Scheme 2) as well as in the calculated dipole moments, that is, 3.39 D for the $^3B_2$ state and 3.28 D for the $^1B_2$ state.[11] The second excited singlet state ^1A (excitation energy of 0.97 eV) has a nonplanar geometry.[12] To a first approximation, the electronic structure of the ^1A state can be described as that of an ionic state (Scheme 2), which is also reflected by the much larger dipole moment of 5.70 D. The high electron density located on the oxygen atoms makes the ^1A state the best candidate for protonation. The ground state of singly protonated *meta*-benzoquinone $\mathbf{8}^+$ is a singlet and correlates with the ^1A state of neutral *meta*-benzoquinone; the triplet state is 0.32 eV higher in energy. Upon twofold protonation resulting in $\mathbf{9}^{2+}$, the singlet ($^1A_1$) and the triplet ($^3B_2$) states come close in energy. The UB3LYP/cc-pVTZ calculations predict the triplet state of $\mathbf{9}^{2+}$ as the electronic ground state with the singlet only 0.04 eV higher in energy. Finally, even though *meta*-benzoquinone (**7**) prefers a different electronic structure ($^3B_2$, $^1B_2$) to the *para* and *ortho* isomers (each $^1A_1$), single and double protonation of *meta*-benzoquinone preferentially stabilize those states that are analogous to the ground states of *para*- and *ortho*-BQH^+ and BQH_2^{2+} ($^1A'$ and $^1A_1$, respectively).

Unimolecular reactivity: The metastable ion mass spectra of singly protonated *para*-, *ortho*-, and *meta*-benzoquinones ($\mathbf{2}^+$, $\mathbf{5}^+$, and $\mathbf{8}^+$, respectively) are dominated by the loss of CO (Table 4). This process is associated with a considerable release of kinetic energy, such that the corresponding peaks appear as if they were split into doublets (cf. Figure 1a). The associated kinetic energy release, which indicates a reverse activation barrier, can be estimated from the horn-to-horn distance as 170 meV for the *para* isomer. At first sight, this behavior of $\mathbf{2}^+$ resembles the unimolecular reactivity of neutral *ortho*- and *para*-benzoquinones, whose main primary process upon thermal decomposition is decarbonylation.[13,14] Although *meta*-benzoquinone (**7**) has not been prepared, alkyl-substituted analogues have been proposed as intermediates in the oxidation of resorcinol derivatives and are assumed to also undergo rapid decarbonylation.[15]

To obtain insight into the decarbonylation mechanism, relevant parts of the potential-energy surfaces of the *para* isomers in its various charge states were calculated. Decarbonylation of neutral *para*-benzoquinone **1** (Figure 2) starts with a ring contraction to yield the bicyclic structure **10** with an associated barrier of 3.54 eV. Part of the energy profile along this reaction path is depicted in Figure 3 in more detail. The transition structure TS**1**/**10** corresponds to the cleavage of the C1–C6 bond concomitant with the formation of the bicyclic structure. On the side of the product, the IRC calculation first leads to structure **10***, which is a five-membered ring with a CO group attached almost perpendicular

© 2005 Wiley-VCH Verlag GmbH & Co. KGaA, Weinheim

Table 4. Fragments in the metastable ion mass spectra of cations ($\mathbf{2}^+$, $\mathbf{5}^+$, and $\mathbf{8}^+$) and dications ($\mathbf{3}^{2+}$, $\mathbf{6}^{2+}$, and $\mathbf{9}^{2+}$).[a,b]

	$\mathbf{2}^+$	$\mathbf{5}^+$	$\mathbf{8}^+$	$\mathbf{3}^{2+}$[e]	$\mathbf{3a}^{2+}$[e]	$\mathbf{3b}^{2+}$	$\mathbf{6}^{2+}$[e]	$\mathbf{6a}^{2+}$[e]	$\mathbf{6b}^{2+}$	$\mathbf{9}^{2+}$[e]	$\mathbf{9a}^{2+}$[e]	$\mathbf{9b}^{2+}$
dications												
$[M-H^{\bullet}]^{2+}$				6								
$[M-D^{\bullet}]^{2+}$					5	4		4	6		3	2
$[M-H_2O]^{2+}$				20		1	75		3	18	2	7
$[M-HDO]^{2+}$					3	19		9	68		14	13
$[M-D_2O]^{2+}$					25			81			14	
$[M-CO]^{2+}$	100[c]	100[c]	100[d]	14	16	13	18	19	31	14	18	17
monocations												
$[M-H_3O]^+$				1			12			3		
$[M-H_2DO]^+$						2			11			2[g]
$[M-HD_2O]^+$					2			12			2	
$[M-COH]^+$				100		47[f]	100		50[f]	100		63[f]
$[M-COD]^+$					100	53[f]		100	50[f]		100	37[f]
$[M-CH_3O_2]^+$				4			14			4		
$[M-CH_2DO_2]^+$						6			14			4
$[M-CHD_2O_2]^+$					5			16			5	
$[M-C_5H_5O]^+$				5		3	5		3	6		2
$[M-C_5H_4DO]^+$					6	3		7	3		7	3

[a] Intensities correspond to integrated peak areas; base peak normalized to 100. [b] Signals corresponding to singly charged parent ions that are formed by charge exchange between the dications and background gas have been detected as well. The intensity is in the range 1–3%. [c] Additional loss of C_3H_4 (<0.5%). [d] Additional losses of C_3H_4 (2.5%), C_2H_2O (1.3%), and C_2H_4O/CO_2 (0.5%). [e] The naturally abundant ^{13}C dication precursor was employed in the measurements; the intensities are accordingly corrected for the $^1/_6$ contribution of the isotopologs. [f] The signals overlap, the ratio was determined from opposite horns of overlapping doublets. For the sake of comparison, the sum of $[C,O,H]^+$ and $[C,O,D]^+$ losses was set to 100; see also text and Figure 1c. [g] The number corresponds to the sum of intensities of H_2DO^+ and H_3O^+ losses.

(89°) with respect to the plane of the ring. However, this structure does not represent a stationary point, and geometry optimization leads to minimum **10**. We have extensively searched for a symmetrical transition structure that could imply a cheletropic expulsion of CO from **1**. However, the only low-energy saddle-point found, TS**10**/**10**′ (E_{rel}=2.76 eV), corresponds to a stereo-isomerization between **10** and its mirror image **10**′. Attempts to localize a symmetrical stationary point (either a first- or second-order TS) between **1** and TS**10**/**10**′ failed. Single point calculations reveal, however, that the energies of structures between **1** and TS**10**/**10**′ are high and even exceed those of TS**1**/**10**. Hence, a low-energy pathway for a symmetrical cheletropic decarbonylation is excluded.

Finally, intermediate **10** releases carbon monoxide as it passes through TS**10**/**11** (E_{rel}=2.22 eV), which leads to the formation of cyclopentadienone (**11**). This scenario is in agreement with the mechanism deduced from kinetic studies of *para*-benzoquinone pyrolysis.[13,14] The barrier associated with dissociation into CO and cyclopentadienone was estimated as 2.6 eV; note that this value is based on pyrolysis at 1550–1900 K.[13] For comparison, the relative free energy of TS**1**/**10** at 1800 K (ΔG) amounts to 3.22 eV. Although an increase of temperature decreases the barrier height, the energy difference between experimental and calculated values remains significant. This discrepancy might be ascribed to the neglect of other reaction channels in the experiments which also liberate CO, for example, decarbonylation of the cyclopentadienone.[14]

The mechanism of decarbonylation of singly protonated *para*-benzoquinone $\mathbf{2}^+$ (Figure 4) also commences with formation of a bond between the carbon atoms 2 and 6. The corresponding barrier (TS$\mathbf{2}^+$/$\mathbf{12}^+$, 2.25 eV) is more than 1 eV lower than for the neutral quinone **1**. The intermediate $\mathbf{12}^+$ further decomposes by passing through TS$\mathbf{12}^+$/$\mathbf{13}^+$ (E_{rel}=1.06 eV) to *O*-protonated cyclopentadienone $\mathbf{13}^+$ and CO. Similar to neutral *para*-BQ, the search for a transition structure corresponding to a cheletropic expulsion of CO leads to TS$\mathbf{12}^+$/$\mathbf{12}'^+$, which represents yet another degenerate isomerization. Mechanisms involving intermediates with seven-membered rings have been examined as well, but all structures considered lie substantially higher in energy than their counterparts with five-membered rings. Hence, mechanisms proceeding through intermediates with seven-membered rings do not contribute significantly to the CO elimination process. A comparison of the mechanisms for *para*-benzoquinone and singly protonated *para*-benzoquinone thus leads to the conclusion that the overall reactivity and the course of the rearrangements are qualitatively similar. Protonation, however, facilitates both the ring contraction as well as the expulsion of CO. A simple interpretation could arise from the fact that protonation withdraws electron density from the ring and thus, the C–C bond to be broken during the ring contraction is weakened. This line of reasoning is also supported by a lengthening of the respective C–C bonds in $\mathbf{2}^+$, that is, 1.49 versus 1.44 Å.

The unimolecular fragmentations of doubly protonated benzoquinones BQH_2^{2+} are not as selective as those observed for their singly protonated counterparts (Table 4). Nevertheless, the dominant signal corresponds to charge separation resulting in the formation of $[C,O,H]^+$ (5%) and $[C_5,H_5,O]^+$ (100%).[16] In comparison with the decarbonylation of BQH^+, the expulsion of $[C,O,H]^+$ from BQH_2^{2+} proceeds with an even larger kinetic energy release due to Coulomb explosion,[17,18] which manifests itself as a well-resolved doublet peak in the MI spectrum (Figure 1b). The kinetic

 © 2005 Wiley-VCH Verlag GmbH & Co. KGaA, Weinheim

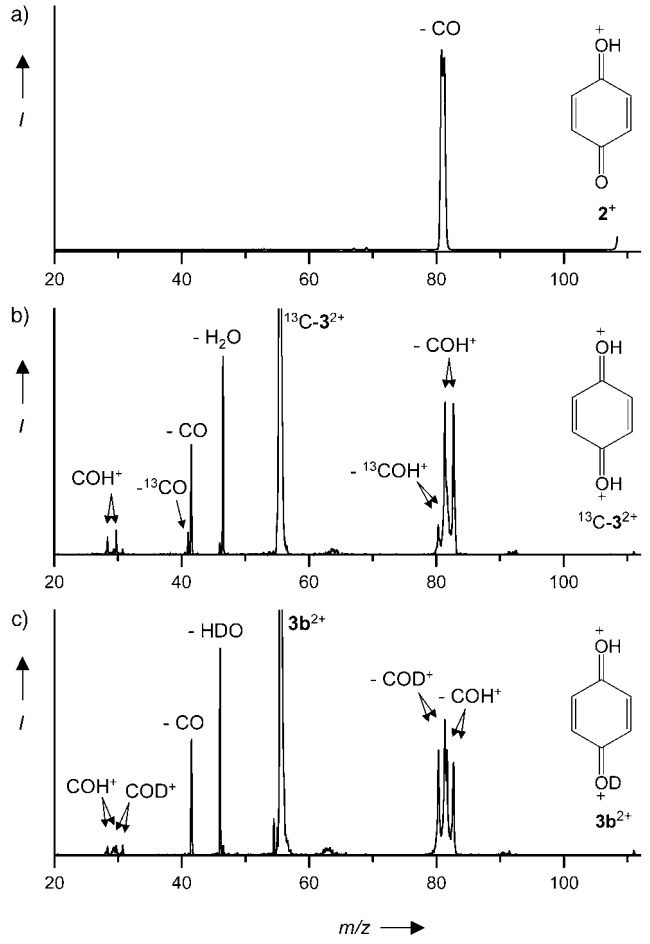

Figure 1. MI spectra of a) singly protonated *para*-benzoquinone $\mathbf{2}^{+}$, b) doubly protonated *para*-benzoquinone $\mathbf{3}^{2+}$, and c) the mono-deuterated analogue $\mathbf{3b}^{2+}$. Due to overlapping isobaric monocationic fragments, the naturally abundant ^{13}C precursor of $\mathbf{3}^{2+}$ was employed in the measurements. Note that the abundances given in the text and the tables refer to integrated peak areas rather than heights. Further, the signals of the precursor dication are off scale in b and c.

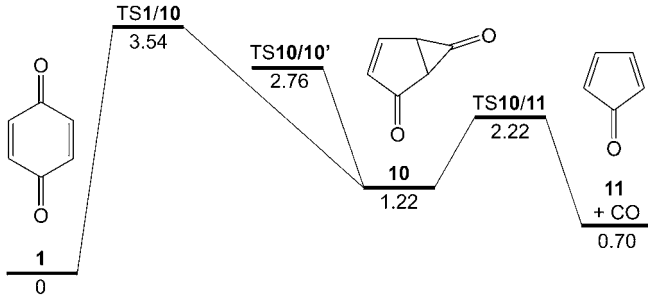

Figure 2. Reaction pathway corresponding to the decarbonylation of *para*-benzoquinone **1** (relative energies are given in eV).

energy release associated with $[C,O,H]^{+}$ expulsion from *para*-BQH_2^{2+} is estimated from the horn-to-horn distance to be 3.4 eV. Other fragmentations correspond to losses of neutral molecules, namely H_2O (intensity 20%) and CO (14%); note that integrated peak areas rather than peak heights are considered.

The MI spectrum of *O,O*-dideuterated *para*-benzoquinone ($\mathbf{3a}^{2+}$, *para*-BQD_2^{2+}) provides further insight into the reaction mechanism. Exclusive formation of $[C,O,D]^{+}$ as well as its loss are observed, thus demonstrating that charge separation is not preceded by H/D exchange processes. With regard to the unlabeled compound, this finding implies that either the COH^{+} fragment is expelled without prior rearrangement of the hydroxyl-hydrogen atom (which, on the other hand, would lead to the more stable HCO^{+} isomer),[19,20] or hydrogen migration occurs specifically to the carbonyl carbon. Overall, the abundances of neutral losses (CO 16%, D_2O 25%, HDO 3%) are slightly increased with respect to the expulsion of $[C,O,D]^{+}$. The preferential elimination of D_2O suggests a specific rearrangement of deuterium associated with little hydrogen scrambling, rather than a ring-walk mechanism for which rapid H/D equilibration is expected.[21] To obtain the intramolecular kinetic isotope effect (KIE), the mixed-labeled compound **3b** (*para*-BQHD—only one hydroxyl function is labeled with deuterium) was examined as well. Despite the partial overlap of the doublets corresponding to the losses of $[C,O,H]^{+}$ and $[C,O,D]^{+}$, the relative ratio can be determined from the opposite horns as approximately 1:1.13 (Figure 1c). The inverse KIE suggests a more complicated reaction mechanism than might have been anticipated. Either the elimination of $[C,O,H]^{+}$ ($[C,O,D]^{+}$) is accompanied by a hidden hydrogen rearrangement from the other hydroxyl group,[22] or the competition of several channels finally leads to an inverse KIE for the competitive $[C,O,H]^{+}/[C,O,D]^{+}$ elimination. The relative intensities of neutral molecule losses are in the range as for the unlabeled compound (CO 13%, HDO 19%, H_2O 1%).

The structure of the $[C,O,H]^{+}$ fragment was probed by comparison of the CA spectra of the $[C,O,H]^{+}$ ions formed in the ion source from hydroquinone (**3**) and formaldehyde, respectively; the latter serves as a reference compound that preferentially yields HCO^{+}.[23] The relative abundances of C^{+}:CH^{+}:O^{+}:OH^{+} are 2.4:1:0.9:0.7 for $[C,O,H]^{+}$ generated from hydroquinone and 1.3:1:0.6:0.2 for $[C,O,H]^{+}$ generated from formaldehyde. The CH^{+} fragment is assumed to originate from HCO^{+}, whereas the OH^{+} ion preferentially comes from the COH^{+} isomer. The signal for OH^{+} is more than three times larger in the spectrum of $[C,O,H]^{+}$ from hydroquinone than in the spectrum of $[C,O,H]^{+}$ from formaldehyde. Accordingly, a non-negligible amount of the thermochemically less stable oxygen-protonated CO, that is, COH^{+}, is formed upon dissociative EI of hydroquinone; this assignment can also account for the specific formation of COD^{+} from $\mathbf{3a}^{2+}$. The decisive experiment, a MI/CA spectrum of the $[C,O,H]^{+}$ fragment formed from metastable $\mathbf{3}^{2+}$, was however impossible on intensity grounds.

The MI spectra of the metastable dication of resorcinol $\mathbf{9}^{2+}$ and its isotopologues are similar to those of the *para* isomer. The spectrum of the unlabeled dication (*meta*-BQH_2^{2+}) is dominated by $[C,O,H]^{+}$ loss along with elimina-

© 2005 Wiley-VCH Verlag GmbH & Co. KGaA, Weinheim

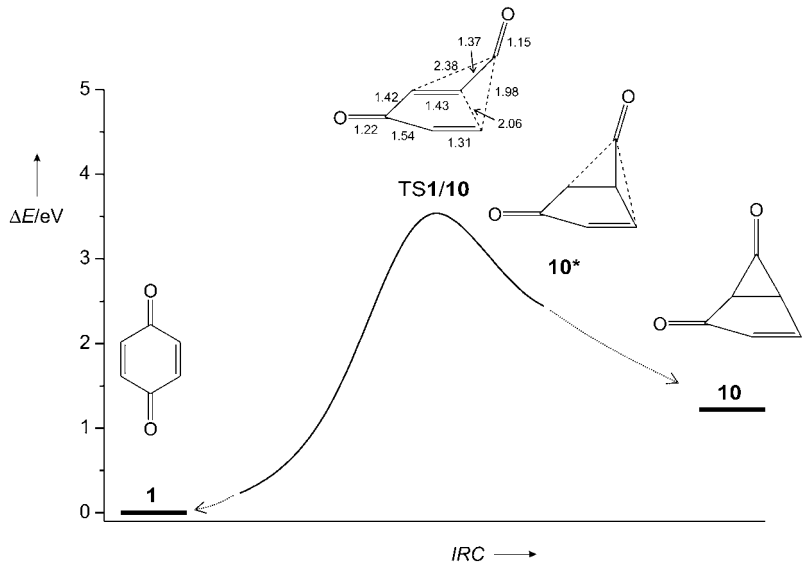

Figure 3. Representative part of energy profile along the IRC for the rearrangement of **1** to **10** (UB3LYP/6–31G**). Some bond lengths (in Å) of TS**1**/**10** are given. The IRC calculations only covered the range given as full line; the dotted connections to the related minima are tentative.

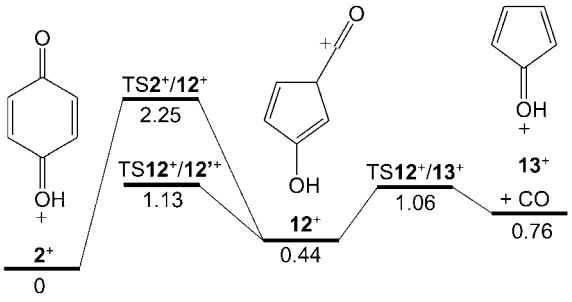

Figure 4. Reaction pathway corresponding to the decarbonylation of singly protonated *para*-benzoquinone $\mathbf{2}^+$ (relative energies are given in eV).

tions of the neutral molecules CO (14%) and H_2O (18%). Besides $[C,O,D]^+$, the *O,O*-dideuterated dication $\mathbf{9a}^{2+}$ loses CO (18%), D_2O (14%), and HDO (14%). The cation radical of resorcinol $\mathbf{9}^{\bullet+}$ is known to undergo keto–enol tautomerization between the OH groups and the adjacent CH groups,[24] prior to decomposition. The analogous process can also be responsible for the hydrogen scrambling in the dication $\mathbf{9a}^{2+}$. To a first approximation, the initial hydrogen scrambling (prior to fragmentation) is more than 50% as estimated from the ratio of D_2O:HDO:H_2O = 7.5:7.5:1. The spectrum of the mixed-labeled dication $\mathbf{9b}^{2+}$ (*meta*-BQHD) is listed as well for the sake of completeness, but the insight into the KIE is limited due to hydrogen scrambling.

The MI spectrum of metastable *ortho*-BQH_2^{2+} ($\mathbf{6}^{2+}$) is somewhat different. This can be attributed to the operation of an *ortho*-effect.[25] The most intense peak still corresponds to the $[C,O,H]^+$ loss. However, the spatial proximity of the OH groups increases the eliminations of H_2O (75%) and of H_3O^+ (12%). The abundance of decarbonylation (18%) is similar to that observed for the *meta*- and *para*-isomers. Labeling of the hydroxy groups with deuterium ($\mathbf{6a}^{2+}$) brings again the same apparent KIE in that the eliminations of CO (19%), D_2O (81%), HDO (9%), and HD_2O^+ (12%) are somewhat more abundant compared to the expulsion of $[C,O,D]^+$. The mixed-labeled dication $\mathbf{6b}^{2+}$ eliminates $[C,O,H]^+$ and $[C,O,D]^+$ in approximately a 1:1 ratio. Another peak that appears in the MI spectra of all isomers, but which is more pronounced for the *ortho*-isomer, corresponds to the loss of $[CH_3O_2]^+$. Upon labeling ($\mathbf{6a}^{2+}$), a mass shift by two units, and thus the elimination of $[CHD_2O_2]^+$, is observed. Most probably, this fragment arises from a sequential fragmentation to yield either $H_3O^+ + CO$ or $H_2O + [C,O,H]^+$. This view of the $[CH_3O_2]^+$ expulsion is consistent with the fact that this channel is more pronounced for the *ortho* isomer, for which H_2O and H_3O^+ losses are significantly more abundant. The proposed mechanism was further tested by investigating the MI spectra of the intermediate fragment ions. The most abundant signal in the MI spectrum of $[\mathbf{6}^{2+}-H_2O]$ corresponds to the loss of $[C,O,H]^+$. Similarly, the dominant fragmentation of $[\mathbf{6}^{2+}-H_3O^+]$ is due to elimination of neutral CO. On the other hand, the ion $[\mathbf{6}^{2+}-COH^+]$ almost exclusively decomposes by loss of CO and no H_2O elimination has been detected. The MI spectrum of $[\mathbf{6}^{2+}-CO]$ contains a signal corresponding to H_3O^+ loss, but there is a more abundant process that leads to the elimination of $C_2H_3^+$.

The interpretation of the unimolecular reactivities of doubly protonated benzoquinones in comparison with those of neutral and singly protonated benzoquinones is again based on theoretical investigations and, as above, restricted to the *para* isomer $\mathbf{3}^{2+}$. A mechanism which is formally analogous to the decarbonylation pathways proposed for neutral and singly protonated *para*-benzoquinone is displayed in Figure 5. Although the intermediate $\mathbf{14}^{2+}$ resembles structure **10** to some extent, the detailed mechanisms of the rearrangements differ. Whereas decarbonylation of neutral benzoquinone starts with a cleavage of the C1–C6 bond and a subsequent formation of the C2–C6 bond (Figure 3), the rearrangement of doubly protonated benzoquinone $\mathbf{3}^{2+}$ proceeds first to the bicyclic TS$\mathbf{3}^{2+}$/$\mathbf{14}^{2+}$, which represents a saddle point. The structure of TS$\mathbf{3}^{2+}$/$\mathbf{14}^{2+}$ can be viewed as a complex between π electrons of the ring and CH^+ cation. In the second step the C1–C6 bond is cleaved by the simultaneous formation of the C2–C6 bond (Figure 6). This proc-

 © 2005 Wiley-VCH Verlag GmbH & Co. KGaA, Weinheim

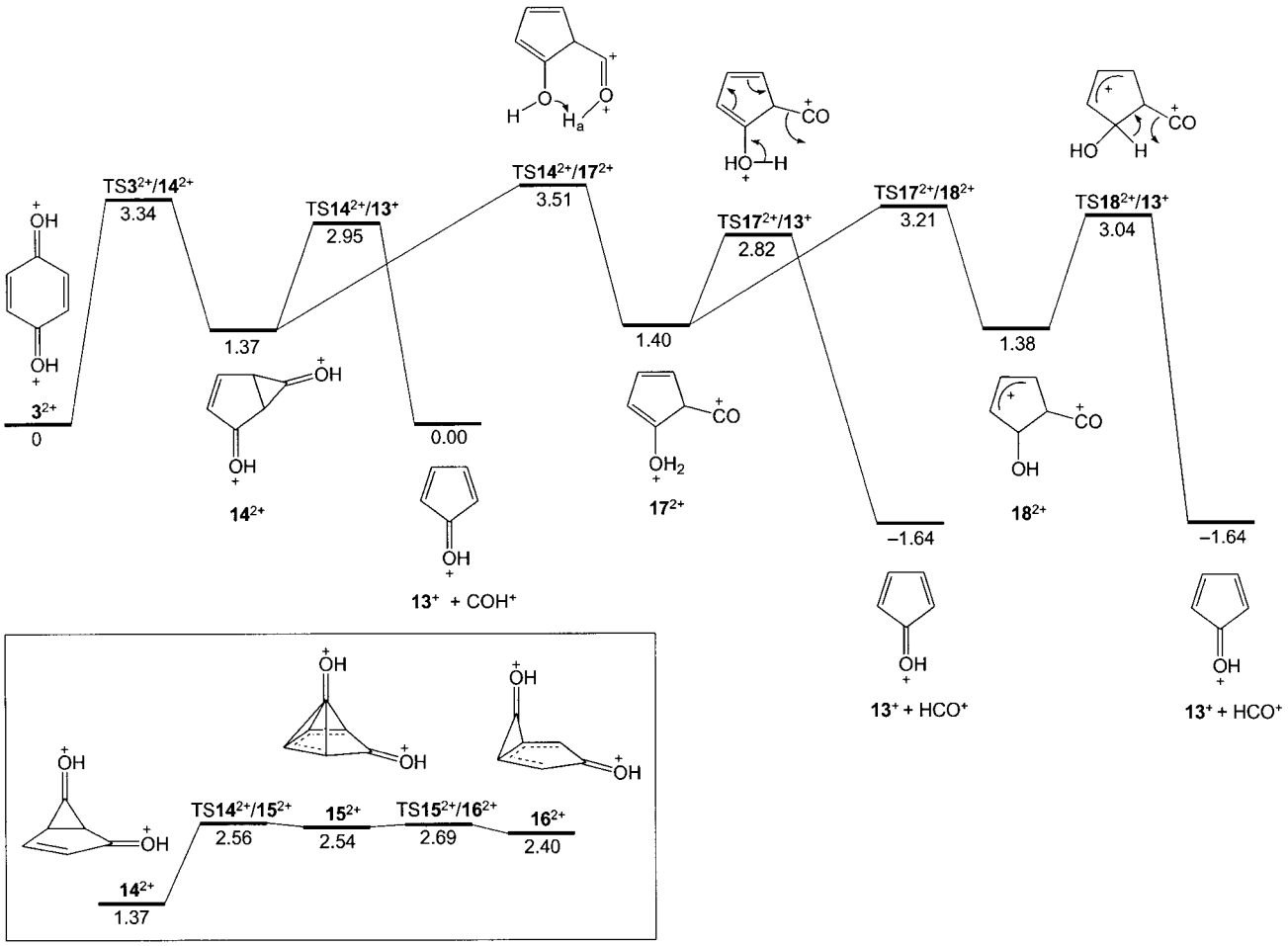

Figure 5. Reaction pathways corresponding to the decarbonylation of doubly protonated *para*-benzoquinone $\mathbf{3}^{2+}$ through five-membered intermediates (relative energies are given in eV).

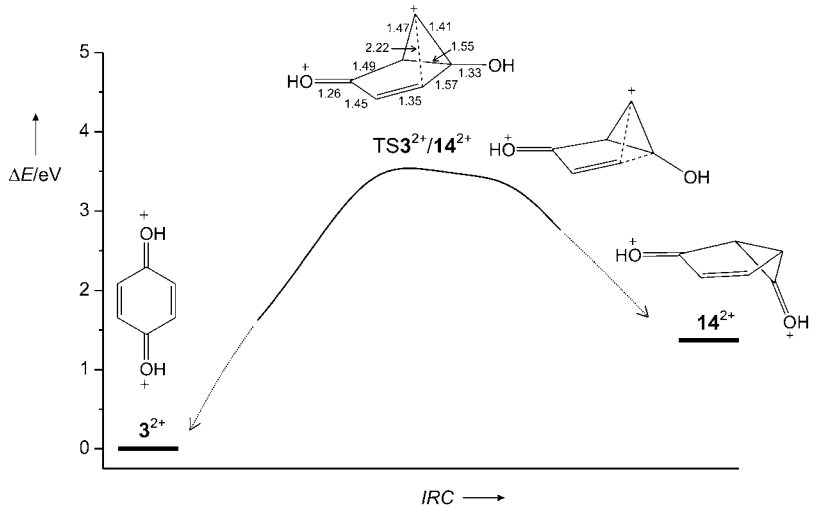

Figure 6. Representative part of energy profile along the IRC for the rearrangement of $\mathbf{3}^{2+}$ to $\mathbf{14}^{2+}$ (UB3LYP/6–31G**). Some bond lengths (in Å) of TS$\mathbf{3}^{2+}$/$\mathbf{14}^{2+}$ are given. The IRC calculations only covered the range given as full line; the dotted connections to the related minima are tentative.

© 2005 Wiley-VCH Verlag GmbH & Co. KGaA, Weinheim

ess is associated with a barrier of 3.34 eV. The "nonclassical" nature of TS3^{2+}/14^{2+} recurs also in structures of 15^{2+} and 16^{2+},[26] which provide a route for a degenerate rearrangement of 14^{2+} (inset in Figure 5). These structures can be viewed as π complexes between protonated cyclopentadienone and a COH^+ ion. Such "nonclassical" structures have been inferred for several dications derived from aromatic molecules.[27] In the case of the benzene dication, the symmetrical pyramidal structure represents a global minimum.[28]

The least energy-demanding decomposition of intermediate 14^{2+} proceeds through TS14^{2+}/13^+ (E_{rel} = 2.95 eV) and leads to the elimination of the COH^+ ion and the formation of protonated cyclopentadienone 13^+ (all attempts to find a transition structure which would correspond to a direct dissociation of 15^{2+} or 16^{2+} into cyclopentadienone and COH^+ led also to the transition state TS14^{2+}/13^+). In addition to charge separation, 14^{2+} can also undergo a hydrogen-atom rearrangement passing through TS14^{2+}/17^{2+} (E_{rel} = 3.51 eV). This specific hydrogen migration explains the preferential D_2O elimination from the deuterium-labeled compound $3a^{2+}$. Thus, along the entire reaction pathway the deuterium atoms remain bound to the oxygen atoms and only in the very last step, one deuterium is directly transferred from one oxygen to the other, thereby preventing a scrambling with hydrogen atoms bonded to carbon.[29] Besides other decomposition routes, which will be discussed later, the intermediate 17^{2+} can also release an HCO^+ ion either in one step passing through TS17^{2+}/13^+ (E_{rel} = 2.82 eV) or in two steps through TS17^{2+}/18^{2+} (E_{rel} = 3.21 eV) leading to the intermediate 18^{2+}. This expels the HCO^+ ion by passing through TS18^{2+}/13^+ (E_{rel} = 3.04 eV). Obviously, the second pathway is disfavored, because it involves larger barriers and an additional intermediate.

Instead of contraction to a five-membered ring, an alternative mechanism would involve expansion to a seven-membered ring to yield 22^{2+} (Figure 7). A possible route might proceed through 19^{2+} as an intermediate, but structure 19^{2+} is much too high in energy (E_{rel} = 4.33 eV) and thus, this mechanism appears unlikely. Another plausible rearrangement is sketched in the hypothetical structure [20^{2+}]. Despite an extensive search, however, such a structure could not be located either as a minimum or a saddle point. Instead, a two-step mechanism leading to intermediate 22^{2+} is suggested in Figure 7. The hydrogen atom is transferred to the carbon atom C2 by passing through TS3^{2+}/21^{2+} which requires 3.20 eV and leads to the acyclic intermediate 21^{2+}.

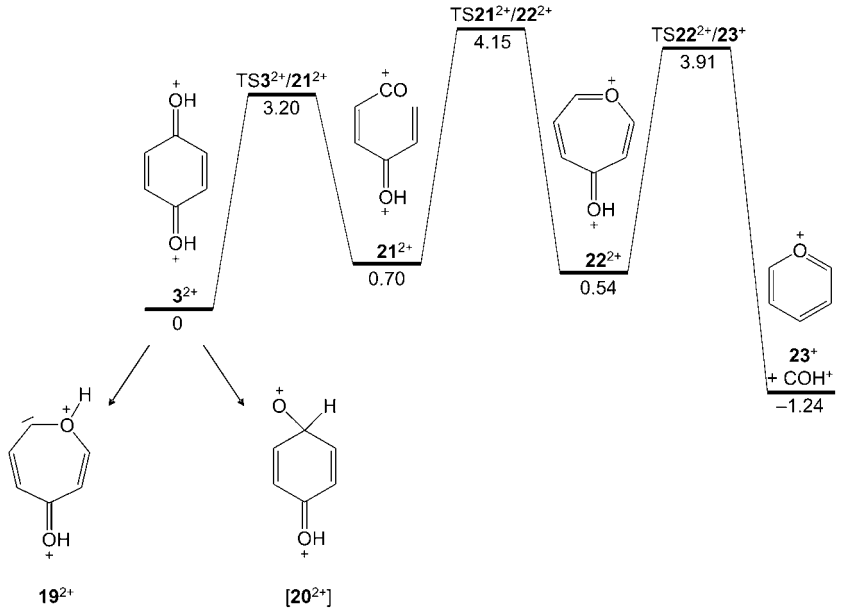

Figure 7. Reaction pathway leading to the decarbonylation of doubly protonated *para*-benzoquinone 3^{2+} through seven-membered intermediates (relative energies are given in eV).

Relaxation of the dication 21^{2+} involves essentially conformational changes that move the methylene group away from the carbonyl group. Thus, further continuation on the way to 22^{2+} will be either connected with a large entropic bottleneck or should proceed without relaxation of the intermediate 21^{2+}. With regard to the large barrier (TS21^{2+}/22^{2+}, E_{rel} = 4.15 eV) associated with the rearrangement to 22^{2+}, it can be expected that intermediate 21^{2+} undergoes relaxation; presumably, 21^{2+} does not release $[C,O,H]^+$ at all. As to the dissociation of the intermediate 22^{2+}, the barrier height (TS22^{2+}/23^+, E_{rel} = 3.91 eV) also appears quite high. Thus, we conclude that even if there would exist more convenient pathways to intermediate 22^{2+}, they most probably do not provide a mechanism which leads eventually to the $[C,O,H]^+$ elimination.

Next, let us address the minor routes that lead to losses of neutral carbon monoxide and water, respectively (Figure 8). Intermediate 17^{2+} is an obvious precursor that can directly eliminate either CO or H_2O. Decarbonylation leads to the product dication 24^{2+} with a relative energy of 3.20 eV. As intermediate 17^{2+} is formed from 3^{2+} with a barrier of 3.51 eV (TS14^{2+}/17^{2+}), it has sufficient internal energy to eliminate a CO molecule.[30] The same argument does not apply for the direct elimination of water, because the corresponding product 25^{2+} is significantly higher in energy (E_{rel} = 4.94 eV). Nevertheless, the H_2O elimination is more abundant for metastable 3^{2+} than the loss of carbon monoxide, which implies that an alternative mechanism exists. A possible pathway proceeds by the 1,5-sigmatropic rearrangement of 17^{2+} to intermediate 26^{2+}. The height of the barrier (TS17^{2+}/26^{2+}, E_{rel} = 2.67 eV) is lower than the energy required for the elimination of CO from 17^{2+} (3.20 eV). It is also lower than the energy required for HCO^+ elimination (TS17^{2+}/13^+, E_{rel} = 2.82 eV). Hence, the rearrangement of

 © 2005 Wiley-VCH Verlag GmbH & Co. KGaA, Weinheim

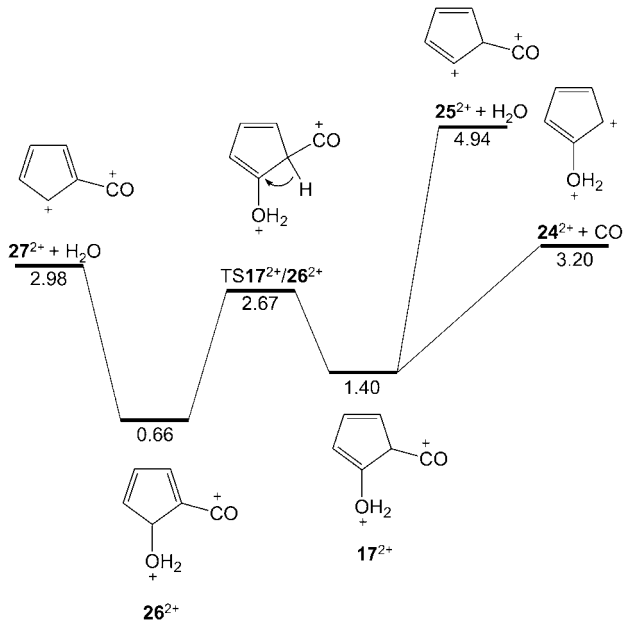

Figure 8. Reaction pathways leading to the eliminations of H_2O and CO from the intermediate $\mathbf{17}^{2+}$ (relative energies are given in eV).

$\mathbf{17}^{2+}$ to $\mathbf{26}^{2+}$ is expected to proceed efficiently. Finally, decomposition of $\mathbf{26}^{2+}$ leads to the formation of a neutral water molecule ($E_{rel}=2.98$ eV).

With regard to the observed KIEs, competition between the different channels is obvious. To estimate the effect of the exchange of hydrogen atoms in $\mathbf{3}^{2+}$ by deuterium in $\mathbf{3a}^{2+}$, the zero-point vibrational energies were also calculated for key-intermediates and transition structures of the respective deuterated analogues. The crucial point concerns the decomposition of intermediate $\mathbf{14}^{2+}$; it can either release COH^+ or undergo rearrangements followed by the elimination of H_2O, CO, or HCO^+. The barrier height for the direct decomposition is 1.58 eV ($E_{rel}(TS\mathbf{14}^{2+}/\mathbf{13}^{+})-E_{rel}(\mathbf{14}^{2+})$). Upon labeling, the barrier increases by only 0.01 eV. On the other hand, the barrier for the rearrangement increases from 2.14 eV ($E_{rel}(TS\mathbf{14}^{2+}/\mathbf{17}^{2+})-E_{rel}(\mathbf{14}^{2+})$) to 2.27 eV, which is a consequence of the fact that deuterium is transferred along this coordinate. This finding provides a rationale for the observed inverse KIE of $\mathbf{3b}^{2+}$. If deuterium were in the "active position" of the hypothetical structure $TS\mathbf{14b}^{2+}/\mathbf{17b}^{2+}$ ($H_a=D$, Figure 5), the barrier ($TS\mathbf{14b}^{2+}/\mathbf{17b}^{2+}$) would be relatively higher and the intermediate would decompose preferentially with the loss of COD^+. On the other hand, when a hydrogen atom migrates ($H_a=H$), a relatively higher fraction of the respective intermediate $\mathbf{14}^{2+}$ undergoes the rearrangement to the intermediate $\mathbf{17}^{2+}$, which, in the end, contributes to the HDO and CO losses. Accordingly, an inverse KIE is indeed expected from the calculations, thereby confirming the experimental observations.

In summary, the $[C,O,H]^+$ ion is most probably eliminated as the less stable COH^+ isomer. The mechanism of its expulsion is analogous to those suggested for decarbonylation of neutral *para*-benzoquinone **1** and the singly protonated molecule $\mathbf{2}^+$, although the initial rearrangement to the five-membered ring proceeds through a different transition structure. This reflects the low electron density in dication $\mathbf{3}^{2+}$. If the key intermediate $\mathbf{14}^{2+}$ does not directly decompose, it can undergo a series of hydrogen rearrangements that finally lead to the eliminations of water, carbon monoxide, and the HCO^+ ion. Although the proposed mechanism has been calculated only for the *para*-isomer $\mathbf{3}^{2+}$, the key intermediate $\mathbf{14}^{2+}$ is expected to be common for the *para*, *ortho*, and also the *meta* isomers. As in the fragmentation of singly protonated benzoquinone $\mathbf{2}^+$, a superficial rationale can be offered for the dication decays: when benzoquinone is doubly protonated ($\mathbf{3}^{2+}$), the positive charge on the oxygen atoms leads to a strong polarization of the C–O bonds and the resulting electron deficiencies of C1 and C4 are compensated for by overlap of π orbitals of the ring resulting in partial multiple bonding character of the C–C bonds to be broken. Accordingly, the activation energies for cleavages of the C–C bonds increase in comparison to that for singly protonated benzoquinone.

The effect of electron delocalization on the fragmentation pattern is particularly illustrated by the *meta* isomer $\mathbf{9}^{2+}$. Although its ground state is a triplet, the MI spectrum of $\mathbf{9}^{2+}$ is almost identical to that of the *para* isomer $\mathbf{3}^{2+}$, which clearly has a singlet ground state. The reason most probably comes exactly from the structure of the triplet state of the dication $\mathbf{9}^{2+}$ (Scheme 2). In contrast to the singlet state, the triplet has strongly delocalized π electrons, thus it can be expected that barriers associated with cleavage of the ring C–C bonds are larger. The calculated relative energies of 3.64 eV and 1.47 eV for the associated transition structures $TS\mathbf{9}^{2+}/\mathbf{14}^{2+}$ (^3A) and $TS\mathbf{9}^{2+}/\mathbf{14}^{2+}$ (^1A) (Figure 9), respectively, perfectly support this scenario. Fragmentation of $\mathbf{9}^{2+}$ then can be explained on the basis of spin interconversion. From the theoretical studies of the phenyl cation[31] and its *para*-substituted derivatives,[32] it has been suggested that the spin isomerization takes place in the region of crossing of singlet

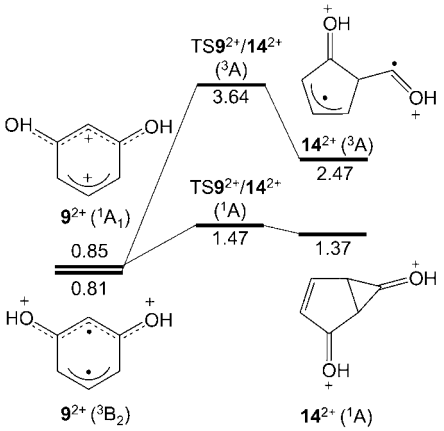

Figure 9. Rearrangement of doubly protonated *meta*-benzoquinone $\mathbf{9}^{2+}$ in triplet $^3B_2$ and singlet $^1A_1$ state (relative energies are given in eV).

© 2005 Wiley-VCH Verlag GmbH & Co. KGaA, Weinheim

and triplet potential-energy surfaces. Minimum energy crossing points (MECPs) of the two surfaces lie either very close in energy to the excited state (for states well separated in energy) or lead to only a small barrier (for nearly-degenerate states). Thus, although the probability of the spin-interconversion might be low, the system passes the MECP frequently, which finally leads to a high overall spin isomerization rate. As the dication $\mathbf{9}^{2+}$ has two almost degenerate states, rapid spin interconversion can be expected. Accordingly, the triplet state is expected to interconvert to the excited singlet state within the μs timescale followed by a sequential dissociation on the singlet surface, rather than a fragmentation occurring on the triplet surface.

Conclusion

Singly protonated benzoquinones decompose in an analogous fashion to neutral benzoquinones by release of a CO molecule. Protonation decreases the electron density in the ring, which facilitates C–C bond cleavage and thus decomposition of the ion. The barrier height of the initial step to CO elimination from *para*-benzoquinone **1** is 3.54 eV and decreases to 2.25 eV upon protonation.

Doubly protonated benzoquinone $\mathbf{3}^{2+}$ releases COH^+ through charge separation instead of CO. It is shown that this process is similar to the decarbonylation of **1** and $\mathbf{2}^+$, except that the released carbon monoxide is protonated. Paradoxically, double protonation again increases the overall barrier height to 3.34 eV. The reason stems from the partial delocalization of π electrons in the ring, which works against C–C bond cleavage.

Although the ground state of resorcinol dication $\mathbf{9}^{2+}$ is a triplet, its MI spectrum only reflects the behavior of the singlet state. The reason is ascribed to the significantly larger barrier for the decomposition of the triplet state ($\Delta E =$ 2.83 eV) relative to the singlet state ($\Delta E = 0.62$ eV). Accordingly, spin-intercorversion is proposed to precede fragmentation.[33]

Experimental Section

The experiments were performed with a modified VG ZAB/HF/AMD four-sector mass spectrometer of BEBE configuration (B stands for magnetic and E for electric sector), which has been described in detail previously.[34] The cations and dications of interest were generated by 70 eV electron ionization of the corresponding neutral precursor molecules and accelerated by a potential of 8 kV (BQH^+ cations were obtained by dissociative ionization of BQH_2, the same spectra were obtained also for BQH^+ cations generated by dissociative ionization of the corresponding hydroxyanisole compounds). The ionization energies of the corresponding monocations were determined from energy-resolved charge stripping (CS) experiments. By virtue of the superior energy resolution of E(1), energy-resolved CS experiments were conducted with B(1)-only mass-selected precursor ions. The mono- and dication signals were scanned at energy resolutions $E/\Delta E \geq 4000$, and Q_{min} values were determined from the differences between the high-energy onsets of the mono- and the dication peaks. The kinetic energy scale was calibrated using CS of the molecular ion of toluene, $C_7H_8^+ \rightarrow C_7H_8^{2+}$ with $Q_{min}(C_7H_8^+) = 14.8 \pm 0.2$ eV[35] using a multiplicative calibration scheme.[36] The unimolecular fragmentations of BQH^+ cations and BQH_2^{2+} dications are monitored by recording metastable ion (MI) mass spectra. To this end, the ions were mass-selected by means of B(1)/E(1) and the unimolecular fragmentations of metastable ions occurring in the field-free region preceding the second magnet were recorded by scanning B(2). The $[C,O,H]^+$ ions were characterized by their collisional activation (CA) mass spectra. To this end, B(1)/E(1) mass-selected ions were allowed to collide with helium (80% transmission) and the fragments arising were scanned by B(2). All spectra were accumulated with the AMD-Intectra data systems; 5–15 scans were averaged to improve the signal-to-noise ratio. Final data were derived from 2–6 independent measurements with an experimental error smaller than ±5%. The averaged spectra were normalized to the base peak which was arbitrarily set to 100%. In order to avoid overlaps in the spectra of dications having even masses ($\mathbf{3}^{2+}$, $\mathbf{3a}^{2+}$, $\mathbf{6}^{2+}$, $\mathbf{6a}^{2+}$, $\mathbf{9}^{2+}$, $\mathbf{9a}^{2+}$) with isobaric monocations, the naturally abundant dications with one ^{13}C atom were employed in the measurements. The intensities given in the Table 4 were accordingly corrected for the $^1/_6$ contribution of the ^{13}C isotopologues.

Computational details: The calculations were performed by using the density functional method UB3LYP[37] in conjunction with Dunning's correlation consistent triple zeta basis set (cc-pVTZ)[38] as implemented in the Gaussian03 suite.[39] For all optimized structures, frequency analysis at the same level of theory was used in order to assign them as genuine minima or transition structures on the potential-energy surface (PES) as well as to calculate zero-point vibrational energies (ZPVEs). All structures were pre-optimized by using the same method but a smaller basis set (UB3LYP/6–31G**), and all transition structures were characterized by intrinsic reaction coordinate (IRC) calculations[40] at this level of theory. Note, however that the PESs involved are quite complex and various other pathways might be considered. Thus, the present calculations are mostly restricted to the *para* isomers and serve as a guide for the interpretation of the experimental data, rather than providing a complete description of the PES. Likewise, we have not considered all possible isomers (e.g. those being formed by 1,2-H shifts) but only those relevant with respect to the fragmentation pathways observed experimentally. Relative energies (E_{rel}) of structures given below are calculated from energies at 0 K and related to **1**, $\mathbf{2}^+$, and $\mathbf{3}^{2+}$, respectively. The electronic energies and energies including ZPVE are given as Supporting Information (Table S1).

Acknowledgement

Continuous financial support from the European Commission (MCInet), the Deutsche Forschungsgemeinschaft, the Fonds der Chemischen Industrie, and the Gesellschaft von Freunden der Technischen Universität Berlin is gratefully acknowledged.

[1] D. Voet, J. G. Voet, *Biochemistry*, 2nd ed., Wiley, New York, **1995**.
[2] E. P. L. Hunter, S. G. Lias, *J. Phys. Chem. Ref. Data* **1998**, *27*, 413–656; see also ref. [4], where PA(*para*-BQ) = 8.31 eV.
[3] S. Patai, Z. Rappoport, *The Chemistry of Quinoid Compounds*, *Vol. II*, *Parts 1 and 2*, Wiley, Chichester, **1988**.
[4] K. K. Irikura, M. Meot-Ner (Mautner), L. W. Sieck, A. D. Fant, J. F. Liebman, *J. Org. Chem.* **1996**, *61*, 3167–3171.
[5] R. C. Fort, Jr., S. J. Getty, D. A. Hrovat, P. M. Lahti, W. T. Borden, *J. Am. Chem. Soc.* **1992**, *114*, 7549–7552.
[6] S. G. Lias, "Ionization Energy Evaluation" in NIST Chemistry WebBook, NIST Standard Reference Database Number 69 (Eds.: P. J. Linstrom, W. G. Mallard), March **2003**, National Institute of Standards and Technology, Gaithersburg MD, 20899 (http://webbook.nist.gov).
[7] M. W. Chase, Jr., *J. Phys. Chem. Ref. Data* **1998**, *9*, 1–1951.
[8] A. Wassermann, *J. Chem. Soc.* **1935**, 828–838.
[9] R. Sabbah, E. N. L. E. Buluku, *Can. J. Chem.* **1991**, *69*, 481–488.

 © 2005 Wiley-VCH Verlag GmbH & Co. KGaA, Weinheim

[10] Note the geometrical similarity with protonated acetone for which the C–O bond length amounts to 1.26 Å.
[11] The results for the $^1B_2$ state should be taken with precaution because the description of an open-shell singlet state with single reference methods like UB3LYP inevitably encounters spin-contamination by the triplet state.
[12] The $^1A_1$ state suggested by Fort et al.,[5] who used the UHF/6–31G* method for the optimization of the geometry, is a second-order saddle point at the UB3LYP/cc-pVTZ level of theory.
[13] P. Frank, J. Herzler, T. Just, C. Wahl, *Twenty-Fifth Symposium (Int.) on Combustion*, The Combustion Institute, Pittsburgh, Pennsylvania, **1994**, 833–840.
[14] M. U. Alzueta, M. Oliva, P. Glarborg, *Int. J. Chem. Kinet.* **1998**, *30*, 683–697.
[15] W. H. Starnes, Jr., D. A. Plank, J. C. Floyd, *J. Org. Chem.* **1975**, *40*, 1124–1127.
[16] Even though charge separation implies that $[C,O,H]^+$ and $[C_5,H_5,O]^+$ are formed in a 1:1 ratio, the lighter fragment ion suffers from significant discrimination effects in detection due to the kinetic energy release in Coulomb explosion; see also: B. A. Rumpf, C. E. Allison, P. J. Derrick, *Org. Mass Spectrom.* **1986**, *21*, 295–299.
[17] D. Mathur, *Phys. Rep.* **1993**, *225*, 193.
[18] D. Schröder, H. Schwarz, *J. Phys. Chem. A* **1999**, *103*, 7385–7394.
[19] W. J. Bouma, P. C. Burgers, J. L. Holmes, L. Radom, *J. Am. Chem. Soc.* **1986**, *108*, 1767–1770.
[20] P. C. Burgers, J. L. Holmes, A. A. Mommers, *J. Am. Chem. Soc.* **1985**, *107*, 1099–1101.
[21] D. Kuck, *Int. J. Mass Spectrom.* **2002**, *213*, 101–144.
[22] H. Schwarz, *Top. Curr. Chem.* **1981**, *97*, 1–31.
[23] A. J. Illies, M. F. Jarrold, M. T. Bowers, *J. Am. Chem. Soc.* **1983**, *105*, 2562–2565.
[24] M. Gerhards, C. Unterberg, S. Schumm, *J. Chem. Phys.* **1999**, *111*, 7966–7975.
[25] H. Schwarz, *Top. Curr. Chem.* **1978**, *73*, 231–263.
[26] The validity of B3LYP calculations on TS**14**$^{2+}$/**15**$^{2+}$, **15**$^{2+}$, TS**15**$^{2+}$/**16**$^{2+}$, and **16**$^{2+}$ was checked by re-optimization and frequency calculation at the MP2/6–311G** level.
[27] a) M. J. S. Dewar, M. K. Holloway, *J. Am. Chem. Soc.* **1984**, *106*, 6619–6627; b) H. Schwarz, *Angew. Chem.* **1981**, *93*, 1046–1059; *Angew. Chem. Int. Ed. Engl.* **1981**, *20*, 991–1003.
[28] K. Krogh-Jespersen, *J. Am. Chem. Soc.* **1991**, *113*, 417–423.
[29] Opening of the three-membered ring of **14**$^{2+}$ concomitant with a 1,2-hydrogen shift from the five-membered ring to the COH group was considered as well. The relative energies of associated barriers amount to 4.16 eV and 4.40 eV, respectively, for opening of the two C–CO bonds. This process was therefore rejected in favor of the direct dissociation by TS**14**$^{2+}$/**13**$^{+}$ or rearrangement through TS**14**$^{2+}$/**17**$^{2+}$. 1,2-Hydrogen shifts are not further considered because it would lead to the scrambling of hydrogen, which was not observed experimentally.
[30] We did not attempt to localize transition structures for the eliminations of the neutral molecules. Generally, the dominant interactions are described by the attractive potentials between the dication and the neutral molecule that finally leads to either barrierless dissociation in excess of the endothermicity or to a very loose transition structure typical for a continuously endothermic dissociation process.
[31] J. N. Harvey, M. Aschi, H. Schwarz, W. Koch, *Theor. Chem. Acc.* **1998**, *99*, 95–99.
[32] M. Aschi, J. N. Harvey, *J. Chem. Soc. Perkin Trans. 1* **1999**, *2*, 1059–1062.
[33] H. Schwarz, *Int. J. Mass Spectrom.*, and references therein, in press.
[34] R. Srinivas, D. Sülzle, T. Weiske, H. Schwarz, *Int. J. Mass Spectrom. Ion Proc.* **1991**, *107*, 369–376.
[35] J. Roithová, D. Schröder, J. Loos, H. Schwarz, H.-C. Jankowiak, R. Berger, R. Thissen, O. Dutuit unpublished results.
[36] K. Lammertsma, P. von R. Schleyer, H. Schwarz, *Angew. Chem.* **1989**, *101*, 1313–1335; Angew . *Chem. Int. Ed. Engl.* **1989**, *28*, 1321–1341.
[37] a) A. D. Becke, *J. Chem. Phys.* **1993**, *98*, 5648–5652; b) C. Lee, W. Yang, R. G. Parr, *Phys. Rev. B* **1988**, *37*, 785–789; c) B. Miehlich, A. Savin, H. Stoll, H. Preuss, *Chem. Phys. Lett.* **1989**, *157*, 200–206; d) S. H. Vosko, L. Wilk, M. Nusair, *Can. J. Phys.* **1980**, *58*, 1200–1211.
[38] R. A. Kendall, T. H. Dunning, Jr., R. J. Harrison, *J. Chem. Phys.* **1992**, *96*, 6796–6806.
[39] M. J. Frisch, G. W. Trucks, H. B. Schlegel, G. E. Scuseria, M. A. Robb, J. R. Cheeseman, J. A. Montgomery, Jr., T. Vreven, K. N. Kudin, J. C. Burant, J. M. Millam, S. S. Iyengar, J. Tomasi, V. Barone, B. Mennucci, M. Cossi, G. Scalmani, N. Rega, G. A. Petersson, H. Nakatsuji, M. Hada, M. Ehara, K. Toyota, R. Fukuda, J. Hasegawa, M. Ishida, T. Nakajima, Y. Honda, O. Kitao, H. Nakai, M. Klene, X. Li, J. E. Knox, H. P. Hratchian, J. B. Cross, C. Adamo, J. Jaramillo, R. Gomperts, R. E. Stratmann, O. Yazyev, A. J. Austin, R. Cammi, C. Pomelli, J. W. Ochterski, P. Y. Ayala, K. Morokuma, G. A. Voth, P. Salvador, J. J. Dannenberg, V. G. Zakrzewski, S. Dapprich, A. D. Daniels, M. C. Strain, O. Farkas, D. K. Malick, A. D. Rabuck, K. Raghavachari, J. B. Foresman, J. V. Ortiz, Q. Cui, A. G. Baboul, S. Clifford, J. Cioslowski, B. B. Stefanov, G. Liu, A. Liashenko, P. Piskorz, I. Komaromi, R. L. Martin, D. J. Fox, T. Keith, M. A. Al-Laham, C. Y. Peng, A. Nanayakkara, M. Challacombe, P. M. W. Gill, B. Johnson, W. Chen, M. W. Wong, C. Gonzalez, J. A. Pople, Gaussian 03, Revision A.1, Gaussian, Inc., Pittsburgh PA, **2003**.
[40] a) C. Gonzalez, H. B. Schlegel, *J. Chem. Phys.* **1989**, *90*, 2154–2161; b) C. Gonzalez, H. B. Schlegel, *J. Phys. Chem.* **1990**, *94*, 5523–5527.

Received: July 19, 2004
Published online: December 2, 2004

© 2005 Wiley-VCH Verlag GmbH & Co. KGaA, Weinheim